Control of a Variable Speed Generator to Optimise Output from a Heaving Wave Energy Device

K.S. Lok, T. Stallard and P. K. Stansby
School of Mechanical, Aerospace and Civil Engineering, University of Manchester, UK
k.lok@student.manchester.ac.uk

Abstract

This study investigates the power generation system and control of an isolated wave device in which heave oscillation of a float drives a flywheel which in turn rotates the shaft of an induction generator. This represents a single unit within a "Manchester Bobber" wave power device; a concept which comprises a closely spaced array of heaving floats. The hydrodynamics have been tested at several scales, 1:100th and 1:70th scale in university test facilities and at 1:10th scale in a large outdoor test tank to evaluate a non-linear model of device response. However, limited research has been undertaken on the power generation system or on control in order to maximise energy extraction from irregular wave-fields. In particular it is important to understand how the torque-speed curve of the generator influences performance and loading. To this end, a model has been developed using EMTDC (ElectroMagnetic Transient including DC) to simulate the coupled electro-mechanical system of a single drive-train when subject to irregular wave-forcing. This is a development of a model of the float hydrodynamics and mechanical system (by Stansby et al.) in which the generator was modelled as a constant torque machine.

Sensitivity of device performance to the induction generator torque speed curve is investigated. It is shown that considerable increase of power capture can be obtained by appropriate selection of the generator characteristics but that this is sometimes offset by increased mechanical loads. Specifically, high rates of change of torque may occur. However, these may be reduced by using a proportional-integral controller whilst maintaining similar performance. A brief study of annual output is conducted for a range of sites to assess the variation of performance with deployment location. Finally, an outline of planned experimental validation of these findings is given.

1. INTRODUCTION

The development of devices to generate electricity from ocean waves started, in the UK, in the early 1970's as a potential replacement for fossil fuel power stations to ensure security of energy supplies triggered by the oil crisis [1]. Extensive research into wave energy was conducted during the 1970s to investigate the feasibility of extracting energy from ocean waves and to assess the energy cost if used on a large scale to meet UK demands. Many wave energy devices were developed at this time, and several technologies underwent large-scale testing in the marine environment. Notable devices include the Edinburgh Duck, Flexible Bag, Clam, Japanese OWC amongst many others. Most devices proposed at this time required significant infrastructure for relatively low electrical output. In retrospect, the aims of the research were considered over ambitious. [1].

The concept of shore-mounted oscillating water column (OWC) dominated the design of the 1st generation of wave energy converters (WECs).The main purpose of the 1st generation WECs is to demonstrate their technical feasibility [2][3]. Due to the their deployment locations, they have the advantages of easy and simple construction, open access to maintenance, no need for sub-sea transmission cables and reduced survivability requirements relative to offshore sites due to attenuation of storm waves. However, the energy available to the device is much lower than that in the off-shore region and tidal-range may be larger.

Subsequently, developers moved their interest to install the devices offshore as a much greater amount of energy can be converted by off-shore devices, since the waves have higher energy flux in deep water. In addition, wave energy converters can be deployed in array, so being able to capture greater quantities of energy under certain conditions [4]. Another difference to the first generation WECs is the use of a smaller primary converter such as the point absorbers. These devices possess an advantage of having a high ratio of potentially converted power to device volume, which may increase the project feasibility due to the reduction in capital cost.

Point absorbers have a relatively narrow bandwidth compared to that in other types of WEC with large horizontal extension, such as terminator and attenuator types [5]. Since the wave climate is spread over a wide range of frequencies, a point absorber would normally operate off resonance. Therefore, control methods are typically required to adjust the response to optimise output in irregular waves [6]. The latching technique has received considerable research attention [5][6][7] - states about the latching control, [2][8][9] - for demonstrating the applications of control techniques, but is not straightforward to implement in practice since advance knowledge of the incident wave-train is required. In addition, latching control is only possible if an external force can be arbitrarily specified [7], such a system was used by e.g. AWS, etc [10]. For these reasons stated above, a slightly different approach is considered here in which power device motion is restricted intermittently by connection to a unidirectional generator.

The wave energy converter based on an induction generator is modelled in this paper using EMTDC. The mechanical and hydrodynamic system of the device is based on an earlier model written in FORTRAN [11].

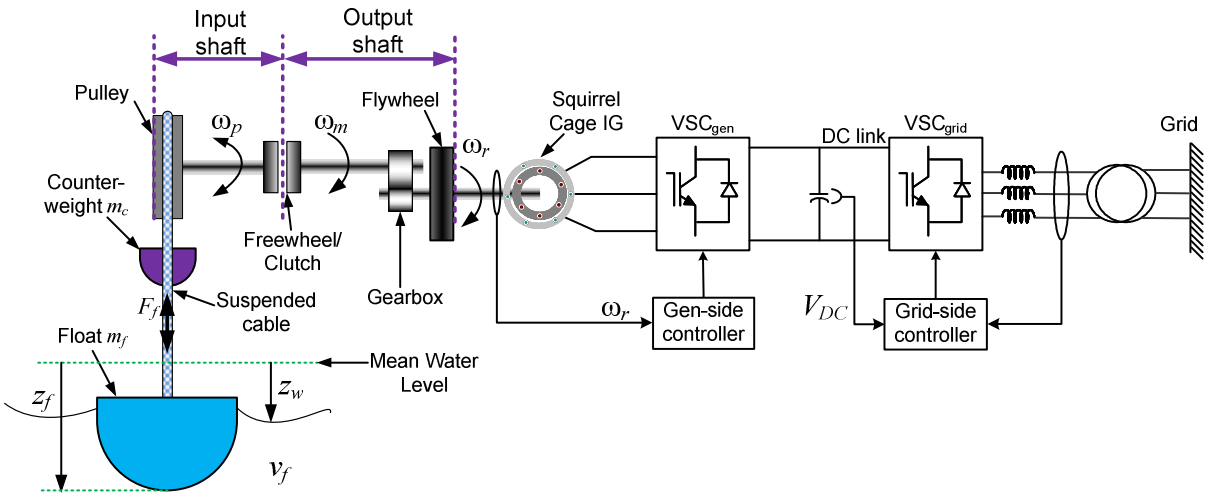

Figure 1. Main mechanical and electrical components of a Manchester Bobber drive-train.

The electrical system is simplified to a 1st order representation and a static characteristic similar to that used in wind-turbine design is shown to be suitable for controlling the device. Two drive-train parameters are optimised for maximising the output power. Finally, it is shown how the use of a proportional integral control method can reduce high rates of change of electromagnetic torque that may otherwise cause damage to the system.

2. MANCHESTER BOBBER

The main components of a single Manchester Bobber drive-train are illustrated in Figure 1. A hemi-spherically ended float of mass m_f and 5 m radius is connected to a pulley by a supporting cable. The other end of the supporting cable connects to a counter-weight m_c, which is always above water. This counter-weight is used to maintain the tension on the cable and provides control over the natural frequency of the device. The float experiences vertical motion due to the excitation force from waves and the resulting force F_f is transmitted through the supporting cable causing oscillatory rotation of the input shaft, ω_p.

As widely used for modelling offshore structures, the wave induced forces F_{fk} on the float are modelled using the Froude Krylov approximation for loading due to the undisturbed pressure field with estimates for added mass and damping added [11]. Scattered waves are neglected but the variation of buoyancy with float displacement relative to the free surface is included based on the continuously changing submerged volume of the float and viscous force is represented in a similar manner to the Morison equation. To ensure that the float oscillates along a vertical axis, a tethering system is employed. This provides an additional vertical restoring force F_{tether} which varies with float displacement z. The force transmitted through the suspended cable F_f is equal to the resolved vertical forces. Although the effects of any scattered waves are ignored these are expected to be small and comparisons to experimental measurements at between 1:100th and 1:10th scale indicate the approach is reliable [11].

After the free-wheel, the oscillatory rotation of the input shaft ω_p is converted to uni-directional rotation ω_m on the output shaft. This uni-direction rotation is geared up (by a ratio of 20 to 1 in this study) to the generator shaft speed ω_r. When the float is descending (positive z direction), the free-wheel clutch will be engaged. The input and output shaft become connected and the whole drive-train starts to accelerate whereas those shafts will be separated when the free-wheel is disengaged. The free-wheel engagement is determined by,

$$\omega_p \geq \omega_m \rightarrow \text{Engaged}$$
$$\tau_c \leq 0 \rightarrow \text{Disengaged}$$

where τ_c is the torque transmitted through the free-wheel.

Under this arrangement, the output shaft will continue to rotate in its forward direction whilst the clutch is disengaged but decelerates at a rate, a_D, determined by the system inertia, J, and the rate of energy extraction (i.e. the power output) during the free-wheel disengaging period according to:

$$a_D = -\frac{\tau_e + \tau_l + \tau_{fw}}{J} \qquad (1)$$

where τ_e is the electromagnetic torque applied to the generator, τ_l is the friction torque in the drive-train, τ_{fw} the friction torque of free running free-wheel.

As shown in Figure 1, the induction generator is connected to the power network through a variable frequency converter system that controls the speed of the generator and the power flowing to the grid. The converter system consists of two IGBT-based back-to-back voltage source converters (VSCs) coupled with a DC link in the middle. This configuration allows the generator to be decoupled from the power network therefore the electrical frequency of the generator can vary as the sea-state changes even though the network frequency is fixed at 50Hz [12].

As seen in Figure 1, the system is divided into two sub-systems; the mechanical system on the left and electrical system on the right. The mechanical system is modelled in EMTDC (ElectroMagnetic Transient including DC) and based upon the earlier model written in FORTRAN, in which a simple generator model was assumed and shown to provide reasonable agreement with 1:70th scale

experimental measurements [11]. Figure 2 shows the simulations of the output power from different generator models. The graph contains the outputs from a 5th-order model, 3rd-order model and 1st-order model. A disturbance is applied at t = 0.2 s and removed at t = 0.35 s. It is seen that the 5th-order model and 3rd-order model oscillate at 50 Hz and 9 Hz respectively whilst recovering from the disturbance but no oscillations are observed in the 1st-order model. However, the output powers from the models are the same when the transient has decayed. Since oscillations within the mechanical system occur at frequencies less than 1 Hz (typically around 0.1 Hz), high frequency oscillations are not expected to affect device performance. In view of this a 1st-order generator model is employed for computational efficiency.

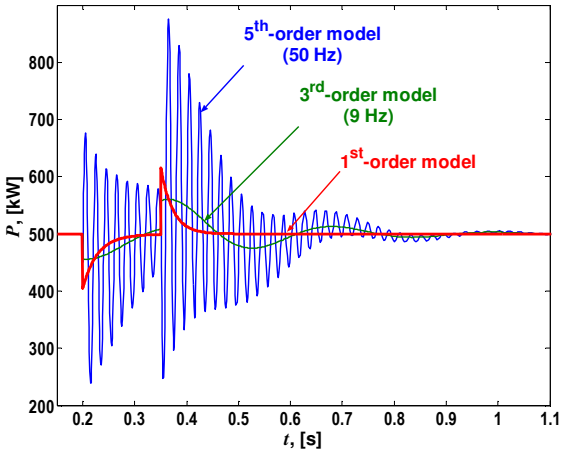

Figure 2. Comparison of output power from generator models of 1st, 3rd and 5th order [13].

Figure 3 (excluding the static characteristic) shows the simplified mechanical representation of the electrical system. The induction generator and its converter are represented in the Laplace domain. The forward loop gain, which includes generator poles p, system inertia J and integrator in Laplace domain $1/s$, combines with the difference between mechanical torque τ_m and electromagnetic torque τ_e to give the rotor speed of the generator ω_r. The output power from the generator P is the product of the rotor speed ω_r and generator electromagnetic torque τ_e.

3. STATIC CHARACTERISTIC

In this control strategy, a system parameter is measured and fed to a look-up table to obtain the required control action. Static characteristic control is used in many applications in the wind industry and for high voltage direct current (HVDC) [14][15][16]. The system configuration and the 1st order representation for the generator and its controller are shown in Figure 3.

The generator rotor speed ω_r is on-line measured and fed through the static characteristic to get the electromagnetic torque reference τ_{ref}. This reference value will be used to calculate ω_r and output power P as illustrated in Figure 3. The shape of the maximum power

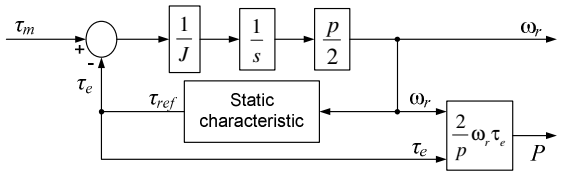

Figure 3. Simplified generator model with static characteristic.

curve used in wind energy is derived from the power co-efficient curve, which describes the relation between the tip speed ratio (the relative velocity of the turbine tip to the wind speed) and the power developed by the turbine [14]. However, this approach is not straightforward to apply to the wave-energy system studied here since wave power is dependent on several parameters and the relationship of these to device power capture is not clearly defined. Therefore, the approach taken here is to investigate a simple torque-speed curve that is similar to the static characteristics used for wind turbines. A static characteristic is shown in Figure 4 and can be considered in three regions; the first region is define by,

$$\tau_{ref} = K \frac{\omega_r}{\omega_{rate}} \tau_{rate} \qquad (2)$$

where ω_{rate} is the rated speed of the generator. The co-efficient K is defined as the gradient of the ramp-up in τ_{ref} in per-unitised (normalised) value.

$$K = \frac{\Delta \tau_{ref,pu}}{\Delta \omega_{r,pu}} \qquad (3)$$

where $\Delta\tau_{ref,pu} = \Delta\tau_{ref} / \tau_{rate}$ and $\Delta\omega_{ref,pu} = \Delta\omega_{ref}/\omega_{rate}$. The second region is the plateau at the rated electromagnetic torque τ_{rate}. The third is constant power region, where τ_{ref} is decreased according to,

$$\tau_{ref} = \frac{P_{rate}}{\omega_r} \qquad (4)$$

such that the rated power of the generator is not exceeded.

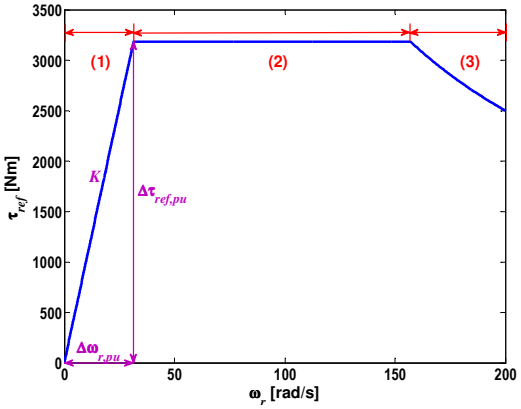

Figure 4. Different regions in the static characteristic.

Regions 1 and 2 are determined by the co-efficient K, which controls the rate of change of τ_{ref} in region 1 and consequently determines the extent of region 2. For K<1, τ_{ref} never reaches τ_{rate} and region 2 vanishes. Figure 5 depicts a simulation run to show the electromagnetic torque and output power from two different values of K

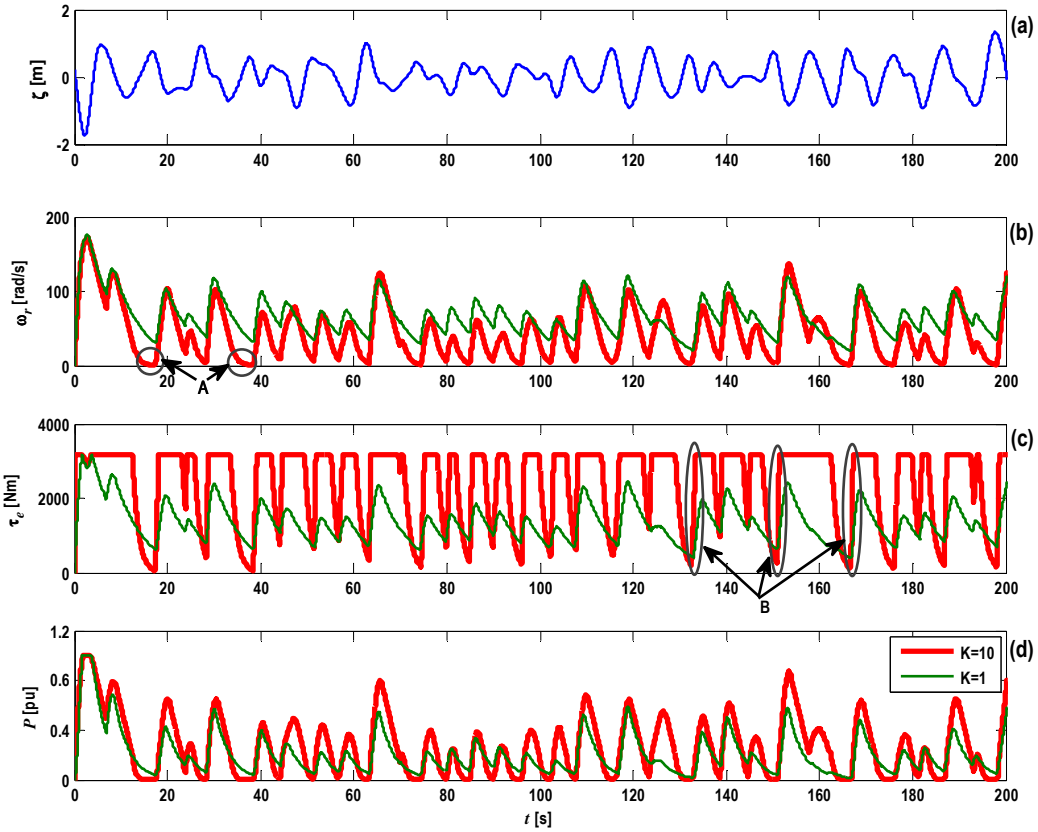

Figure 5. Time variation of (a) incident wave-field defined by JONSWAP spectrum with H_s = 2m and T_p = 10s measured at float centreline, (b) angular speed of generator, (c) generator torque and (d) power output $P = \tau_m \omega_m$ for two values of static characteristic gradient. For K = 1 (thin line) average power output P_{av} = 92 kW and maximum rate of change of torque $d\tau_{e,max}/dt$ = 8 kNm/s whereas for K = 10 (thick line) P_{av} = 126 kW and $d\tau_{e,max}/dt$ = 30 kNm/s.

during an irregular sea-state. The wavefield shown corresponds to a JONSWAP spectrum defined by:

$$S(f) = \frac{\alpha g^2}{(2\pi)^4 f^5} \cdot \exp\left[-\frac{5}{4}\left(\frac{f_p}{f}\right)^4\right] \cdot \gamma^r \qquad (5)$$

$$\text{where } \alpha = 16.9\left(\frac{H_s}{gT_g^2}\right)^{1.375} \qquad (6)$$

$$\text{where } r = \exp\left[-\frac{(f-f_p)^2}{2\sigma^2 f_p^2}\right] \qquad (7)$$

$$\text{with } \sigma = \begin{Bmatrix} 0.07 \leftarrow f \le f_p \\ 0.09 \leftarrow f \ge f_p \end{Bmatrix} \qquad (8)$$

In which H_s=2 and T_p=10 s, f_p is the peak frequency of the spectrum, f is the frequency components within the spectrum, γ is the peak enhancement parameter and having the value of 3.3.

The water surface elevation ζ, in (a), is repeated its pattern at 200s (20 cycles of T_p). To avoid start-up transients, the average power P_{av} and maximum rate of change of electromagnetic torque $d\tau_{e,max}/dt$ are calculated from a 200 s sample after the simulation has run for one complete repeat cycle. Stalling of the drive-train (i.e. $\omega_r = 0$) is not desirable since a high torque is required to overcome static friction. This occurs frequently when K = 10 (as highlighted by A in the interval 130 < t < 170s in Figure 5(b)) but is not observed when K=1. The average power P_{av}, in (d), from K=10 is approximately 36% more than that from K=1. However, this power increase is accompanied by an increase of the rate of change of electromagnetic torque $d\tau_{e,max}/dt$ as pointed by B in (c). The maximum rate of change of electromagnetic torque increases by a factor of 3.75 which may damage the device, particularly raising the mechanical stress in the gearbox and the generator rotor. Hence, the optimisation is aimed at increasing P_{av} while keeping $d\tau_{e,max}/dt$ low (here the maximum power occurs when K=10 but the minimum $d\tau_{e,max}/dt$ occurs when K=1).

It is conventional to express the output power in per-unitised (normalised) values, which is defined by:

$$P_{av,pu} = \frac{\text{Average power } (P_{av})}{\text{Generator power rating } (P_{rate})} \qquad (9)$$

where the generator rating in this study is 500kW. The per-unitised average power $P_{av,pu}$ and maximum rate of change of electromagnetic torque $d\tau_{e,max}/dt$ in different sea-states are plotted in Figure 6(a) and (b). It is seen that the per-unit average power $P_{av,pu}$ using K=10 is greater than that in K=1 in the range of 22-49% according to the sea-states considered. However, it is found that the maximum rate of change of electromagnetic torque $d\tau_{e,max}/dt$ is increased with the value of K as illustrated in Figure 6(b). For the remainder of this study, K=5 is used since higher values do not significantly increase power but result in a roughly linear increase of $d\tau_{e,max}/dt$.

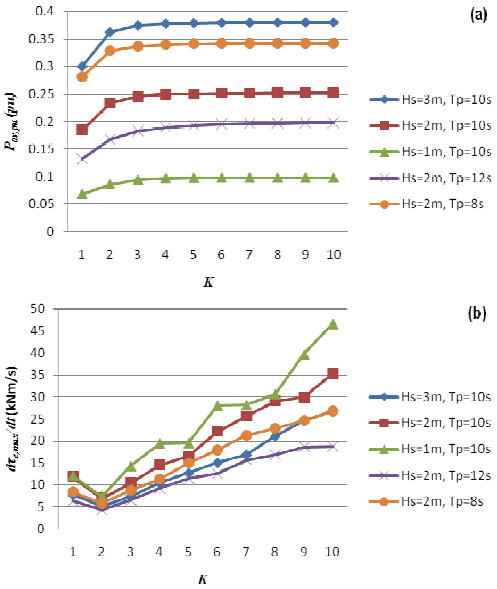

Figure 6. Variation of per-unit average power (a) and maximum rate of change of electromagnetic torque (b) with gradient of static-characteristic (K) for a range of irregular wave-fields.

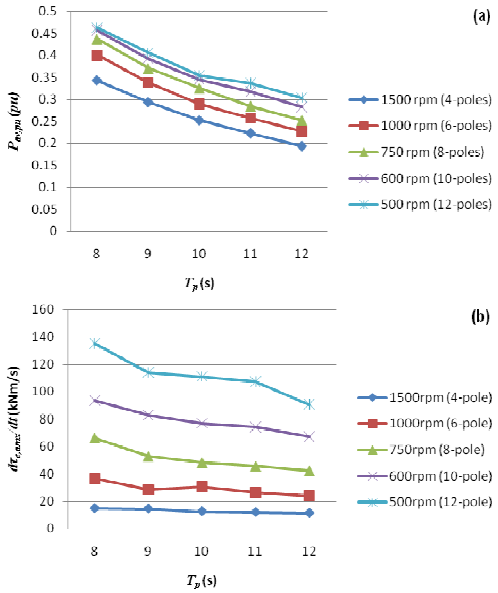

Figure 7. Variation of per-unit average power (a) and maximum rate of change of electromagnetic torque (b) with wave period (H_s=2m) for between 4 and 12 generator poles.

4. PARAMETRIC STUDIES

Two drive-train parameters, the generator poles and flywheel inertia, were varied in order to maximise the average power P_{av} whilst reducing the maximum rate of change of electromagnetic torque $d\tau_{e,max}/dt$.

4.1 Generator Poles

The number of poles in a machine determines the synchronous speed ω_{syn}, which represents how fast the magnetic field rotates in the stator [17][18]. The relation between them is:

$$\omega_{syn} = \frac{4\pi \times f_a}{p} \qquad (10)$$

where f_a is the applied grid frequency in Hz, p is number of poles, ω_{syn} is in rad/s. Since f_a is fixed at 50 Hz, ω_{syn} is inversely proportional to p, which is always an even number. The rated torque τ_{rate} increases when p increases as long as the machine rating is unchanged.

For a flywheel inertia J = 100 kgm^2 and static-characteristic gradient K = 5, Figure 7 shows simulation results of the per-unit average power and the maximum rate of change of electromagnetic torque in various sea-states. It is found that increasing the number of generator poles increases the average power output. However, the higher maximum rate of change of electromagnetic torque $d\tau_{e,max}/dt$ increases with the number of poles. An 8-pole generator seems to be a sensible choice in terms of balance between P_{av} and $d\tau_{e,max}/dt$ as the results suggested in Figure 7.

4.2 Flywheel Inertia

The flywheel functions as short-term kinetic energy storage in the drive-train. The stored energy is particularly useful to keep the rotation of the drive-train in the period of disengaged free-wheel. The rate of drive-train deceleration is dependent on the electromagnetic torque τ_e applied to the generator. Figure 8 shows the per-unit average power and maximum rate of change of electromagnetic torque with different flywheel inertias and sea-states. In the simulations, an 8-pole generator was used and the gain K was kept at 5 while 4 different flywheel inertias were tested.

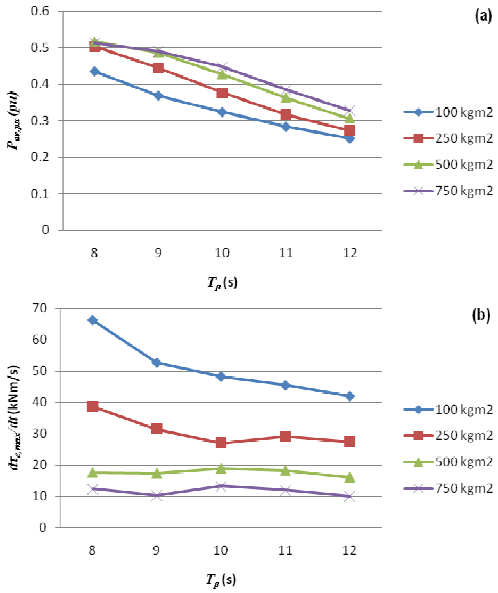

Figure 8. Variation of per-unit average power (a) and maximum rate of change of electromagnetic torque (b) with wave peak wave period (H_s=2m) for a range of flywheel inertias.

A heavier flywheel increases power output and reduces the maximum rate of change of electromagnetic torque. Although a 750 kgm^2 flywheel provides maximum average power, a 500 kgm^2 flywheel, however, has been chosen for an economical reason as illustrated in Table 1. It is assumed that the flywheel is made up of lead, which has density value of 11340 kg/m^3 [19]. A 500 kg/m^2 flywheel is chosen because its performance is only slightly lower than that in a 750 kgm^2 flywheel (shown in Figure 8) but its size and the material needed are 22.5 % less than a 750 kgm^2 flywheel.

Table 1: Dimensions of 0.1 m width lead cylinder flywheel for three inertias

Inertia (kg/m^2)	**100**	**500**	**750**
Radius (m)	0.487	0.728	0.806
Volume (m^3)	0.0744	0.1644	0.204
Weight (ton)	0.844	1.864	2.312

5. PI CONTROLLER

The preceding sections show that by use of a static characteristic and appropriate selection of generator poles and flywheel inertia average power outputs in the range of 0.184 - 0.428pu may be obtained whilst the maximum rate of change of electromagnetic torque is limited to 8-19 kNm/s in the sea-state of H_s = 2m and T_p = 10s. However, the maximum average power is only obtained when the rate of change of torque is high (18 kNm/s at 0.428pu). In this section, it is shown how a Proportional-Integral (PI) controller may be employed to maintain high power output whilst reducing the infrequent but large rates of electromagnetic torque change associated with a static characteristic. The electrical system configuration and the simplified generator model shown with the PI controller are depicted in Figure 9.

The proportional integral controller operates on the difference between the applied electromagnetic torque and the reference electromagnetic torque obtained from the static characteristic for this operating speed. With reference to Figure 9(a), the calculated power P_{calc}, which is the product of the measured instantaneous voltage v and current i across the low voltage side of the transformer, is used to compute the calculated electromagnetic torque τ_{calc}, which is given by,

$$\tau_{calc} = \frac{P_{calc}}{\omega_r} \tag{11}$$

This calculated torque is compared with the reference electromagnetic torque τ_{ref} to give the value of the error signal $\Delta\tau$ (= τ_{ref} - τ_{calc}), and this is input to the PI controller to determine the applied electromagnetic torque τ_e. The PI controller is treated as a feedback controller driving the system to be controlled with a weighted sum and the integral of the error signal $\Delta\tau$. The controller output is defined as,

$$\tau_e = K_p\left(\Delta\tau(t) + \frac{1}{t_i}\int_{t-t_i}^{t}\Delta\tau(t)\,dt\right) \tag{12}$$

where K_p is proportional gain and t_i is an integral time constant. Figure 10 shows the differences in the static characteristic for an 8-pole generator between presence and absence of PI controller in the system.

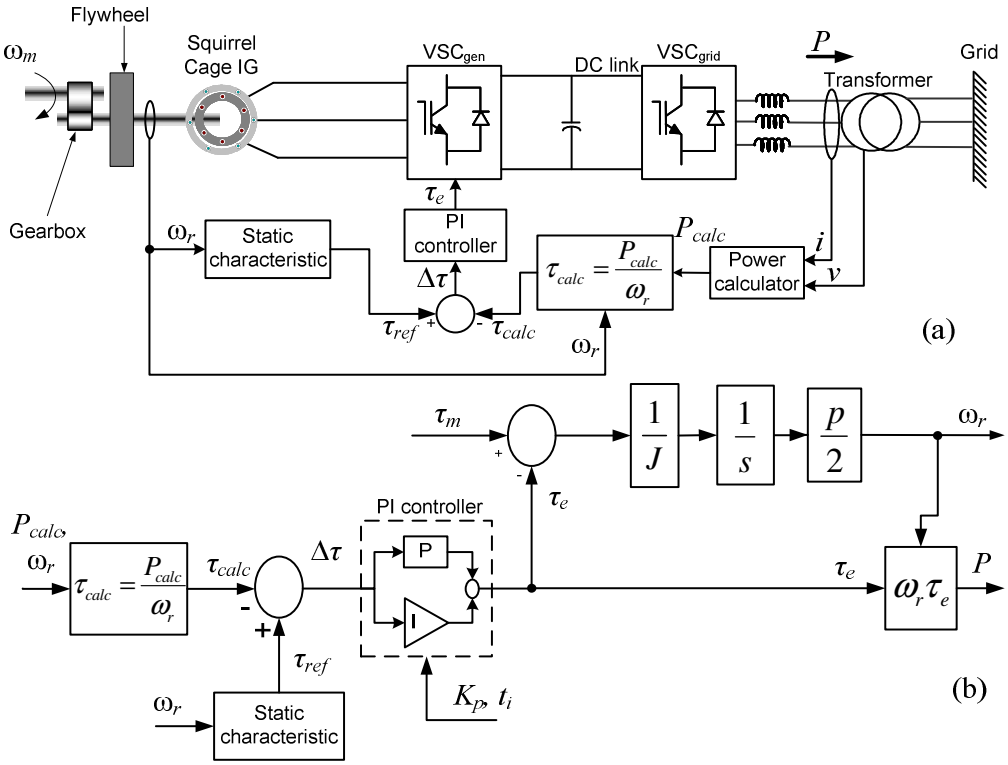

Figure 9. Electrical system configuration (a) and simplified generator model (b) with PI controller.

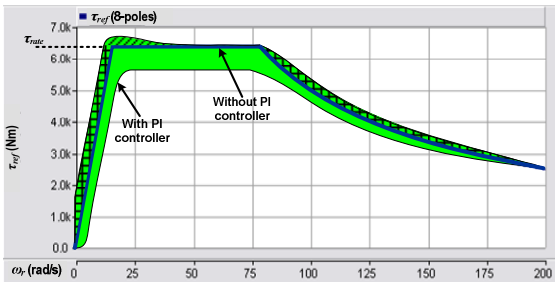

Figure 10. Static characteristic and operating region with proportional integral (PI) controller.

When a PI controller is not used, the system operating point would always be situated on the solid line. However, if a PI controller is used, the system operating point could be located at any point in the shaded region (including the line and square shaded regions above the solid line). The extent of the system operating region is dependent on the PI terms. A fast response PI (small t_i) would have a narrower operating region. Cautions should be given to the slow response PI settings as damages may be caused when the system is operating in the square shaded regions (i.e. above the static characteristic whilst $\omega_r < \omega_{min}$ or $\omega_r > \omega_{rated}$). Operation in the line-shaded region would exceed the rated torque. In general, this is not acceptable since damage will occur and so τ_{ref} is specified as $\tau_{ref} < \tau_{rate}$ to avoid operation in this region.

The PI controller is 'tuned' by adjusting the proportional gain and integral time constant, K_p and t_i. It is found that no significant effect is seen by changing K_p. Therefore, it was kept at 0.01, a low value, throughout the simulations. The simulation results in various PI terms and sea-states are plotted in Figure 11. It is evident that there is no significant reduction of average power output (less than 0.016pu) when the PI controller is included in the system. However, $d\tau_{e,max}/dt$ is dramatically decreased according to the sea-states considered and the PI settings, by between 76% (H_s =2m, T_p = 12s), ($t_i = 0.1T_p$, i.e. the integral time constant equals to 10% of the wave periods considered) and 95% (H_s = 2m, T_p = 8s), ($t_i = 0.5T_p$). This appears to be a feasible method of avoiding torque spikes that may damage the system whilst retaining high average output power.

6. WAVE FIELD SIMULATION

In this section, the numerical model is used to produce a power matrix for the device over the intervals $3<T_p<20$s and $0.25<H_s<6$m. The WEC is supposed to be shut down when H_s is above 6m in order to prevent the device form damages may be caused by severe weather conditions. Two power matrices were produced by utilising the numerical model for two different irregular wave conditions; the first one was generated by using a JONSWAP spectrum (as Equation (5)), which the generated water surface represents wind waves. The second was created by using a Gaussian spectrum, which the water surface represents swell waves.

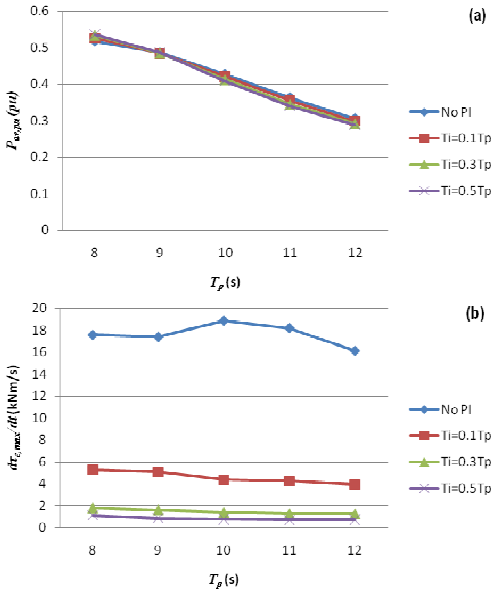

Figure 11. Variation of per-unit average power (a) and maximum rate of change of electromagnetic torque (b) with peak wave period (H_s=2m) for a range of PI integration constants $0<t_i<0.5T_p$.

The annual average power P_{an} at a deployment site is obtained by the product of the device power matrix and the sea-state occurrence matrix.

$$P_{an} = \sum \left(P_{av,pu} \times Q \right) \qquad (13)$$

where $P_{av,pu}$ is the per-unit average power of the corresponding sea-state, Q is the occurrence probability of the corresponding sea-state.

In [20], occurrence matrices are presented for 50 locations within eight different regions around the UK as illustrated in Figure 12. Annual output is evaluated at the eight sites highlighted; one in each region.

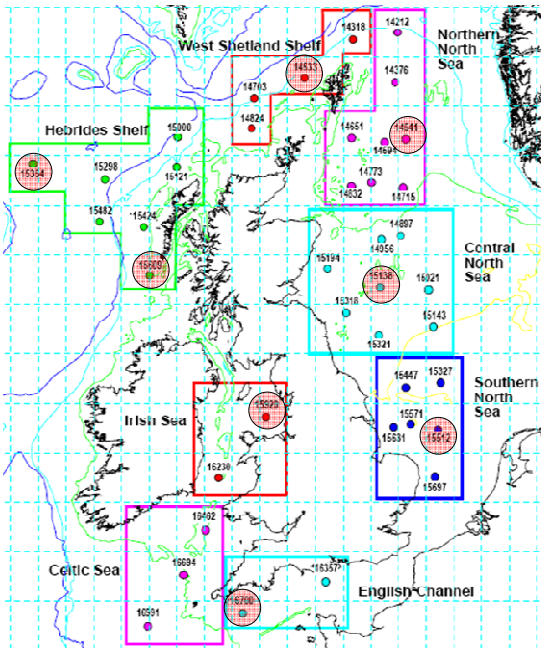

Figure 12. Wave climate data measuring points around the UK [20]

For each location, the annual output from the device is found to be similar when the wave-field is defined by Gaussian, JONSWAP spectra. As might be expected, there is considerable variation of annual output between the sites due to differences in the available resource. The average annual power in average power from different sites is plotted against the average wave height $H_{s,av}$ and average peak wave period $T_{p,av}$.

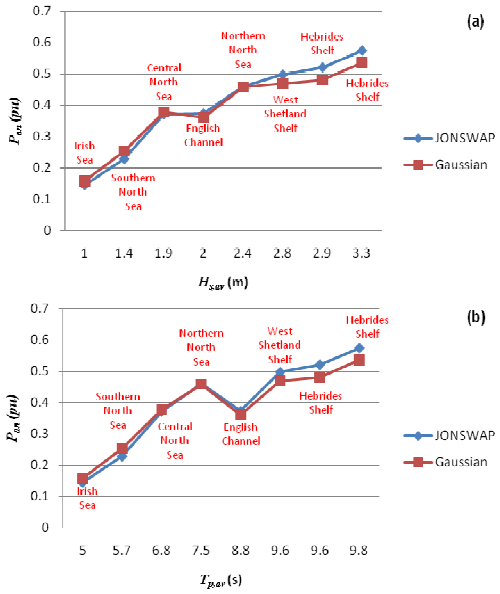

Figure 13. Average annual power from the device using a JONSWAP spectrum and a Gaussian spectrum with average significant wave height (a) and average peak wave period (b).

Figure 13 shows the average annual power from a range of sites when each sea-state is modelled as a JONSWAP spectrum $P_{an,J}$ and a Gaussian spectrum $P_{an,G}$. Each site is represented by the annual average significant wave height $H_{s,av}$ and annual average peak period $T_{p,av}$. It is seen that the average annual power from both spectra are considerably linearly proportional to the average significant wave height $H_{s,av}$. But the deployment site in Central North Sea extracts more power than that in English Channel, even the average wave height $H_{s,av}$ in Central North Sea is actually 0.1 metre lower than that in English Channel. This is because of the average wave period $T_{p,av}$ in Central North Sea is closer to the device resonance period T_0, which the device consequently provides a better performance. In addition, the average annual power using a Gaussian spectrum is slightly higher than that using a JONSWAP spectrum at sites with a frequent occurrence of short period sea-states. Similar outputs are seen around the resonance period. However, the average annual power using a Gaussian spectrum is dropped off compared to the average annual power using a JONSWAP spectrum in long wave periods.

7. CONCLUSIONS

This paper has demonstrated that the static characteristic is a suitable control strategy for the generator of the Manchester Bobber wave energy device. The complete electro-mechanical system is modelled in EMTDC in a range of irregular wave-conditions to assess annual performance. Several parameters have a significant influence on average power output and mechanical loading, these include the generator characteristics, flywheel inertia and control algorithm. It is shown that a significant increase in average power P_{av} is gained by using a generator with more poles and hence a higher rated torque although the performance increase reduces above 8 poles. However, increasing the number of poles also increases the rate of change of electromagnetic torque $d\tau_{e,max}/dt$, which is not desirable. A reasonable balance between output and torque seems to be an 8-pole generator. The flywheel inertia study shows that a heavy flywheel inertia is able to increase P_{av} while reduce $d\tau_{e,max}/dt$; an inertia of 500 kgm^2 was selected to provide a reasonable balance between material needed and performance.

As an alternative to altering the specification of generator or flywheel, the problem of high value of $d\tau_{e,max}/dt$ may be reduced by properly tuning the terms in a Proportional-Integral (PI) controller. The tuning of the PI controller was concentrated on the integral time constant t_i due to no significant effect was found by adjusting the proportional gain K_p. It is shown that, for the system parameters selected, the average output power varies approximately linearly with the annual average significant wave height for a deployment site, although the trend is somewhat non-linear when the average wave period at the site is close to the natural period of the device.

These simulations indicate that a feasible method of controlling the Manchester Bobber power take off system to maximise output whilst avoiding stalling and minimising torque variation is to employ a proportional integral controller to follow a static characteristic. Experimental work is presently in progress to quantify the average power output performance gains suggested.

Acknowledgements

This investigation was funded by the NWDA Joule Centre for Energy Research as part of the first authors PhD studentship. Guidance provided by Prof Nick Jenkins and Dr Alan Williamson regarding electrical machine design is appreciated. The authors are grateful for ongoing support from the industrial partners of the Manchester Bobber project including: Renold Gears, ABB, Offshore Design Engineering (ODE Ltd.), Royal Haskonning, Carillion, Red Rooster, Burnt Island Fabrications (BiFAB), Bridon International.and Renold Chain.

8. REFERENCES

[1]. Thorpe, T.W., (30 November 1999). An Overview of Wave Energy Technologies: Status, Performance and Costs, Wave Power: Moving towards Commercial Viability, Broadway House, Westminster, London.

[2]. Babarit, A. and Clement, A.H. (2006). Optimal latching control of a wave energy device in regular and irregular waves, Applied Ocean Research 28(2) 77-91.

[3]. Boyle, G. Renewable Energy, Power for a Sustainable Future, 2nd edition, Oxford University Press, Oxford, 2004, ISBN: 0199261784.
[4]. Thomas, G.P. and Evans, D.V. (1981). Arrays of three-dimensional wave-energy absorbers J. Fluid Mech. 108 67-88.
[5]. Falnes, J. (2001). Optimum Control of Oscillation of Wave-Energy Converters, Proceedings of the International Offshore and Polar Engineering Conference, 1, 567 -574.
[6]. Salter, S. H., Taylor, J. R. M., and Caldwell, N. J., (2002). Power Conversion Mechanisms for Wave Energy, Proceedings of the IMechE Part M: Journal of Engineering for the Maritime Environment, 216(1), 1-27.
[7]. Falnes, J., (2002). Ocean Waves and Oscillating Systems, Linear Interaction Including Wave-Energy Extraction, Cambridge University Press, Cambridge, UK, ISBN: 0521782112.
[8]. Babarit, A., Duclos, G. and Clement, A.H., (2004). Comparison of latching control strategies for a heaving wave energy device in random sea, Applied Ocean Research, 26(5),227-238.
[9]. Falnes, J. and Bjarte-Larsson, T., (2006). Theoretical and experimental investigation of wave energy conversion by a phase-controlled heaving body", Proceedings of the Institution of Mechanical Engineers, Part M: Journal of Engineering for the Maritime Environment, 220(4), 175-183.
[10]. de Sousa Prado, M.G., Gardner, F., Damen, M. and Polinder, H. (2006). Modelling and test results of the Archimedes wave swing. Proceedings of the Institution of Mechanical Engineers, Part A: Journal of Power and Energy 220 855-868.
[11]. Stansby, P. K., Williamson, A. C., (2006). A simple model to predict power from a heaving point absorber: the Manchester Bobber, Internal report, The University of Manchester.
[12]. Ramtharan, G., Jenkins, N. and Anaya-Lara, O., (2007). Modelling and control of synchronous generators for wide-range variable-speed wind turbines, Wind energy Journal, 10(3), 231-246.
[13]. Caliao, N. D., (2008). Modelling full converter wind turbines, PhD Thesis, School of Mechanical Aerospace and Civil Engineering, The University of Manchester.
[14]. Masters, G. M., (2004). Renewable and Efficient Electric Power Systems, John Wiley & Sons, Inc., Hoboken, New Jersey, ISBN: 0471280607.
[15]. Jenkins N., Strbac, G., Kirschen, D., Allan R. and Crossley, P., (2000). Embedded Generation, IEE Publications, ISBN: 0852967748.
[16]. Aten, M., (2002). HVDC control systems, PhD thesis, Department of Electrical and Electronic Engineering., UMIST.
[17]. Hindmarsh, J., (1984). Electrical machines and their applications, 4th edition, Oxford: Butterworth-Heinemann, ISBN: 0750627948.
[18]. Krause, P.C., Wasynczuk, O. and Sudhoff, S.D, (2002). Analysis of electric machinery and drive systems, 2nd edition, New York : Wiley, ISBN: 047114326X.
[19]. Serway, R.A., Beichner, R.J. and Jewett, J.W.Jr., (2000). Physics for scientists and engineers with modern physics, 5th edition, Fort Worth, Tex.; London: Saunders College, ISBN: 0030226570.
[20]. Fugro GEOS, (2001). Wind and Wave Frequency Distributions for Sites around the British Isles, Offshore Technology Report Series, Health and Safety Executive.